EBG Structure to Improve the B1 Efficiency of Stripline Coil for 7 Tesla MRI

Gameel Saleh[1], Klaus Solbach[1]and Andreas Rennings[2]
[1]High-Frequency Engineering (HFT), [2]General and Theoretical Electrical Engineering (ATE)
University of Duisburg-Essen
Duisburg, Germany

***Abstract*—This paper presents the first application of an EBG structure to improve the *B1* efficiency of strip-line coils used for 7-Tesla Magnetic Resonance Imaging (MRI). The proposed offset multilayer electromagnetic band gap (EBG) structure is utilized as a high impedance surface behind an extended half-wavelength (meandered) dipole. It operates at 300MHz, the magnetic resonance frequency at 7 T, and comprises of electrically small cells of only 7.5% of the free-space wavelength. The reflection phase coefficient and the dispersion diagram were used to characterize the EBG structure. The MRI strip-line coil backed by our EBG structure is successful in exhibiting a stronger B_1-field inside a phantom than the original design using a metallic conductor (PEC) ground plane for the coil. The quantitative improvement in B_1 efficiency amounts to 47%.**

Keywords- B_1-field; electromagnetic band gap (EBG) structures; in-phase reflection band; surface wave suppression band gap; magnetic resonance imaging (MRI) coil; specific energy absorption rate (SAR).

I. INTRODUCTION

Electromagnetic band gap (EBG) structures [1]-[2] are broadly classified as metamaterials due to their unique and useful properties, like the in-phase band gap reflection coefficient, which enables the design of low profile antennas, and the surface wave suppression band gap property, which improves the antenna performance [1].

Transmit arrays for high-field MRI based on loop or strip-line approaches are usually placed above a conducting ground plane (PEC). Thus the RF magnetic flux density (B_1) above the coil (inside the load) is reduced by the anti-phase currents in the PEC ground plane. The novel approach presented in this paper has the objective to improve the B_1 efficiency of a well-established strip-line coil [4] by replacing the PEC ground plane with an EBG structure. Therefore the anti-phase currents can be avoided and the magnetic flux density inside the load is increased. The condition for a successful application of the EBG structure in this application is unique in that the cell dimensions are required to be far below the size of the strip-line structure, which in our case is 25% of the free-space wavelength. Thus, this paper focuses on a multi-layer stacked EBG structure with a lateral cell size of only 7.5% of lambda.

II. PROBLEM FORMULATION AND DESIGN SPECIFICATIONS

When a plane wave illuminates a symmetric EBG surface at normal incidence, the reflection phase is independent of the polarization state, and is stable and can be utilized to define the band-gap feature [1]. The structure can be modeled analytically by using the simple parallel LC resonant circuit [1] as shown below:

$$\omega_0 = \frac{1}{\sqrt{LC}} \tag{1}$$

$$Z = \frac{j\omega L}{1-\omega^2 LC} \tag{2}$$

Where ω_0 is the angular resonance frequency and Z is the surface impedance of the EBG structure. The values of the capacitance C and the inductance L are described in [1].

In this paper, a stacked EBG structure is used, which consists of two arrays of metal patches with a diagonal offset from each other. The top layer is connected to the metal backing of the dielectric substrate by vertical metal-plated vias, while the lower one is floating. The HFSS full wave simulator, based on the FEM algorithm with periodic boundary conditions (PBC) was used to design and characterize one unit cell of the EBG structure, and the FDTD simulator EMPIRE XCcel was used to analyze the finite structure. The geometry of the proposed finite stacked EBG structure together with meander dipole coil over the analyzed structure is shown in Fig 1.

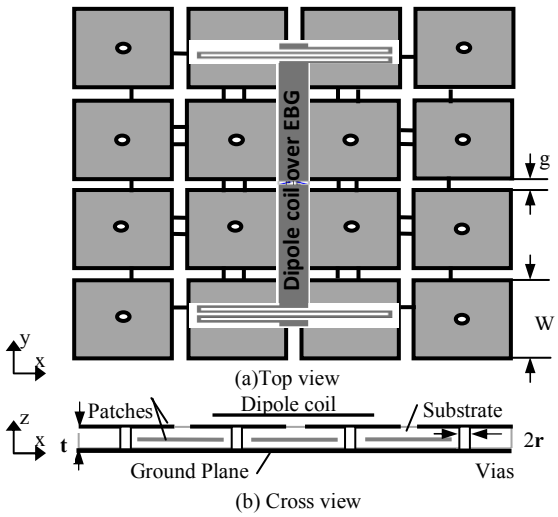

Figure 1. Offset layers stacked EBG design with a meandered dipole

The physical dimensions of the proposed EBG structure are initialized as in (3):

$$W = 0.07475\ \lambda_{300\text{MHz}},\ g = 0.002\ \lambda_{300\text{MHz}},\ t = 0.0064\ \lambda_{300\text{MHz}},$$
$$r = 0.003\ \lambda_{300\text{MHz}}. \quad (3)$$

Where $\lambda_{300\text{MHz}}$ is the free-space wavelength at 300 MHz, which is used as a reference length, W is the patch width, g is the gap width and t is the thickness of the Rogers RO3010 substrate. The spacing between the two layers of patches was chosen to be 0.0032 $\lambda_{300\text{MHz}}$ due to the availability of laminates of 3.2mm thickness. This design has the advantage to provide more capacitive effect, because of the lower copper layer which provides more coupling between the adjacent patches. Therefore it operates at lower frequency than the conventional single layer mushroom EBG structure same way as in [3].

A resonant meandered dipole is used as RF-transmit coil in 7 Tesla MRI (with extended folded arms to resonate at 300 MHz) is mounted on FR4 epoxy substrate of 0.5mm thickness and above the EBG structure such that the total height of the configuration is 20 mm, same as the original coil construction including a PEC ground plane [4].

III. Reflection Phase and Dispersion Diagram

For a plane wave illuminating the proposed EBG surface based on the dimensions given in (3) at normal incidence, the reflection phase is shown in Fig. 2. Our MRI system frequency is in the frequency band where the reflection phase is in the range of $90^0 \pm 45^0$, which was shown to be helpful for low profile wire antennas to achieve good return loss [2].

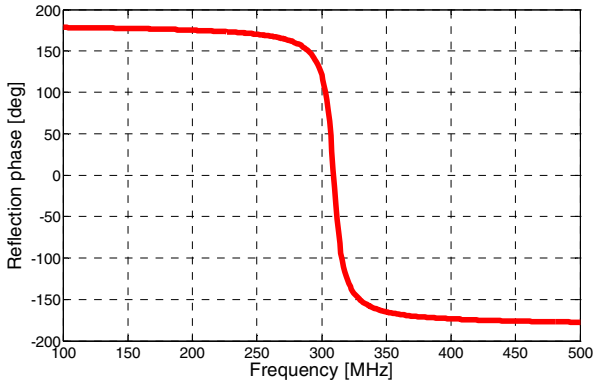

Figure 2. Reflection phase of the proposed EBG structure

Additionally to the reflection phase such an EBG surface can be characterized by its dispersion diagram. This information includes the surface wave characteristics. The dispersion diagram in Fig. 3 shows the importance of vias to prevent a nonzero vertical electric field component to travel between the patch arrays and ground. A surface wave suppression band gap between the first two modes (TM mode and TE mode respectively) is obtained and it has been ensured that our MRI operating frequency in MRI is included within this stop band gap.

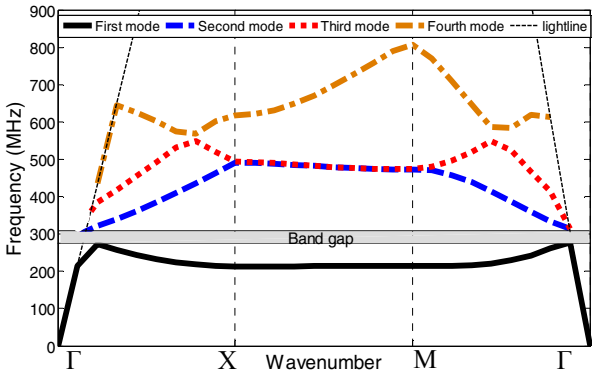

Figure 3. Dispersion diagram of the proposed EBG structure.

IV. Verification of Stop Band Gap Property

In order to validate the simulation result w.r.t. the stop band gap property of the EBG structure, the finite EBG structure was fabricated and was inserted into an air-filled microstrip line test cell. The line was made of a brass sheet of 195mm width which was supported at 40 mm above the ground plane. The microstrip line was connected at both ends to a tapered section connecting to coaxial ports as shown in Fig. 4. Measurement of the microstrip line test cell without the inserted EBG structure exhibited a reflection coefficient at both ports below -18 dB across the 200 to 400 MHz band.

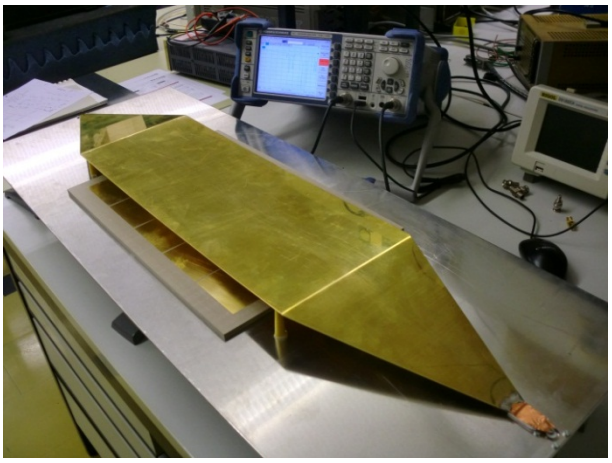

Figure 4. Experimental setup of the microstrip line test cell loaded by the finite EBG structure

A simulation of the insertion loss of the microstrip test cell loaded with the EBG structure was performed in order to allow comparison with measurement. However, during manufacture, the diameter of vias accidentally was changed from 6mm to 3mm and this change was also introduced into the simulation. The simulation used the FDTD simulator-EMPIRE XCcel and assumed the full microstrip test cell with loading by the finite EBG structure applying the same dimensions of both microstrip line as well as EBG structure used as in the measurement. The measurement result is compared to the simulation in Fig. 5. It is seen that the simulated transmission ($S_{2,1}$) coefficient exhibits a number of stop band resonances across the observed bandwidth and this

is well supported by the measurement. Due to the reduced diameter of the vias (increased inductivity), the first stop band gap is found down shifted in frequency, no longer matching our MRI operating frequency. Yet, it is interesting to see that the FDTD simulation result is in an excellent agreement with the measured result as shown in Fig. 5. This correspondence between measurement and simulation results will enable us later to tune the stop band gap of the proposed EBG structure confidently.

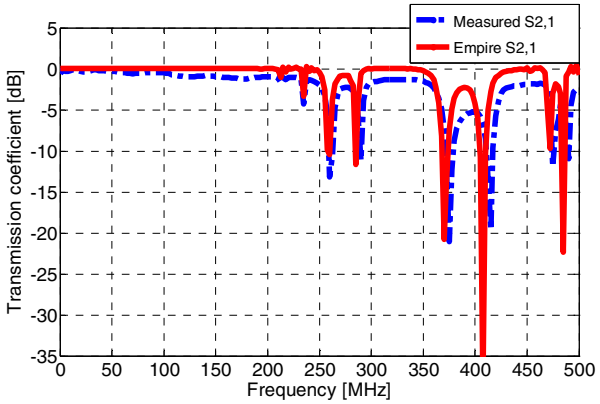

Figure 5. FDTD simulation result and measured transmission ($S_{2,1}$) coefficient of the proposed EBG structure

V. Magnetic Field Inside the Phantom

The performance of the original coil configuration based on a meandered dipole over a PEC ground plane was compared to the performance of the novel design using the EBG structure as a reflector by simulating the magnetic field distribution inside a homogeneous phantom (ε_r = 40, σ = 0.8 S/m) placed 2cm above the coil. In order to compare in fair manner, all values have been normalized to the accepted RF power. The maximum normalized magnetic field intensity in the presence of the proposed EBG structure was 2.266 A/m/√W while the value reduced to 1.538 A/m/√W when a PEC of the same size (305mm X 305mm) is used, i.e. the presence of the proposed EBG structure enhances the B_1-field by about 47% as compared to the PEC case. The distribution of these fields inside the phantom and at different distances along the z - axis is shown in Fig. 6.

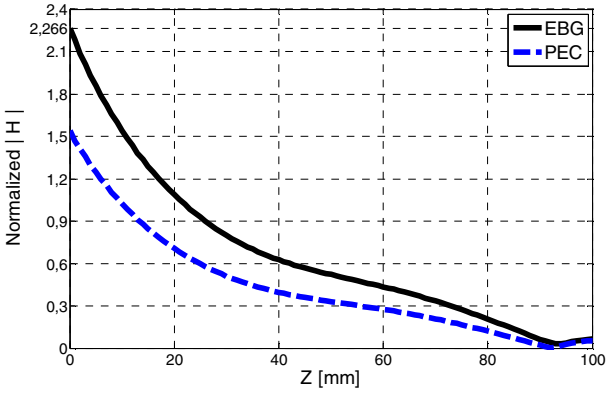

Figure 6. FDTD simulation result for normalized magnetic field inside the phantom along the z-axis

The longitudinal distribution (along y-axis of Fig. 1) of this magnetic field at different heights inside the homogeneous phantom (2cm, 4cm, 6cm, 8cm, and 10cm) when the strip-line coil is backed by the EBG structure is shown in Fig. 7. It is clear from this field distribution that the maximum normalized magnetic field at any height is always at the center, as it also is in the case of the coil over the PEC ground plane. The value of this magnetic field reduces as we go up inside the phantom, as shown in Fig. 6 and 7.

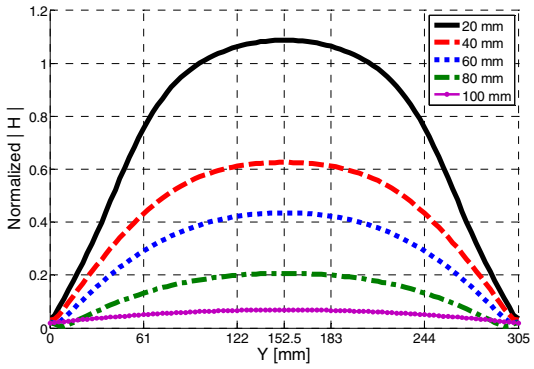

Figure 7. FDTD simulation of longitudinal normalized magnetic field at different height inside the phantom (using EBG structure)

VI. Specific Energy Absorption Rate

The SAR inside the homogeneous phantom at 2cm above the strip-line coil backed by the proposed EBG structure or the PEC ground plane has also been invistigated. All SAR values have been normalized to an accepted RF power of 1W.

In our results the normalized peak localized 10g-based SAR inside the phantom at 2cm above the coil backed by the proposed EBG structure was 3.334 mW/g, while this value reached to 1.518 mW/g in the PEC case. Similar distribution of SAR, yet with increased local and whole-body averaged SAR values have been observed. The increase in the SAR values is assumed to be mainly due to the reflection property exhibited with EBG structure compared to the PEC case, with increase for the electric field as well as for the magnetic field.

The percentage of increase in the √SAR in the EBG structure case over the √SAR in the PEC case is about 48% and this corresponds to the percentage of improvement in the magnetic field and B_1 efficiency.

References

[1] D. Sievenpiper, High-impedance electromagnetic surfaces, PhD dissertation, Dept. Elect. Eng. Univ. California at Los Angeles, Los Angeles, CA, 1999.

[2] Yang, F. and Y. Rahmat-Samii, "Reflection phase characterizations of the EBG ground plane for low profile wire antenna applications," IEEE Transactions on Antennas and Propagation, Vol. 51, No. 10, pp. 2691-2703, 2003.

[3] Yang, F. and Y. Rahmat-Samii, Electromagnetic Band Gap Structures in Antenna Engineering, Cambridge University Press, 2008.

[4] S. Orzada et al., Proc. Intl. Soc. MRM 16 (2008), p.2979